Supporting information

Trinuclear hydride complexes of rhodium

Christian Fischer, Christina Kohrt, Hans-Joachim Drexler, Wolfgang Baumann, Detlef Heller*

Leibniz-Institut für Katalyse e.V. an der Universität Rostock, Albert-Einstein-Straße 29a, 18059, Rostock, Germany, Fax: (+49)-381-1281-51183;phone: (+49)-381-1281-183.

1. Experimental Section

1.1. Synthesis of complexes
1.2. IR-and Raman spectra
1.3.Additional NMR-spectra

2. Crystallographic Section

2.1. Crystallographic experimental section
2.2. Figures of the molecul structures

1. Experimental Section

1.1. Synthesis of complexes

General Information

Chemicals were purchased from Aldrich, Fluka, Strem, CELTICCATALYSTS, Chiralquest and unless otherwise noted were used without further purification. All relevant compounds were characterized by ^{1}H NMR, ^{31}P NMR, ^{103}Rh NMR and if possible HRMS and IR/Raman spectroscopy as well as x-ray analysis of single crystalls.

The NMR spectra were recorded on Bruker ARX-300 or 400 spectrometers. IR spectra were recorded with a Smart Endurance ATR-unit connected with a IR spectrometer Nicolet 6700 (Thermo Fisher). Raman spectrum was recorded on Vertex 70 FT-IR (Bruker). HRMS was performed on Agilent 6210 Time-of-Flight LC/MS (ESI-TOF).

General Synthesis of $\{[Rh(PP^*)H]_3(\mu_2\text{-}H)_3(\mu_3\text{-}H)\}(BF_4)_2$

All experiments were carried out under an argon atmosphere using standard Schlenk technique. (A. Salzer, *Laboratory Techniques of Organometallic Chemistry in Synthetic Methods of Organometallic and Inorganic Chemistry* (Ed. W. A. Herrmann), Georg Thieme Verlag, Stuttgart, **1996**, 8-28.)

The ^{31}P NMR and ^{103}Rh NMR data (figure S3) are summarized in table 2. The ^{1}H NMR spectra were represented in figure 3.

$\{[Rh(Tangphos)H]_3(\mu_2\text{-}H)_3(\mu_3\text{-}H)\}(BF_4)_2$

[Rh(Tangphos)(cod)]BF_4 (0.02mmol) was dissolved in 1 mL MeOH under an argon atmosphere. The argon atmosphere was exchanged by hydrogen and the solution stirred under hydrogen normal pressure for 2.5 h. The solution was then layered with diethyl ether. After a few hours yellow crystals were isolated, which were washed with diethyl ether and dried under vacuum.

MS (ESI-TOF): calc for $\{[Rh(Tangphos)H]_3(\mu_2\text{-}H)_3(\mu_3\text{-}H)\}^{2+}$; ($C_{48}H_{103}P_6Rh_3$): 587.18198; found: 587.18246.

IR: see figure S1.

{[Rh(Me-DuPhos)H]$_3$(μ_2-H)$_3$(μ_3-H)}(BF$_4$)$_2$

The synthesis was carried as for {[Rh(Tangphos)H]$_3$(μ_2-H)$_3$(μ_3-H)}(BF$_4$)$_2$.

MS (ESI-TOF): calc for {[Rh(Me-DuPhos)H]$_3$(μ_2-H)$_3$(μ_3-H)}$^{2+}$; ($C_{54}H_{91}P_6Rh_3$): 617.13503; found: 617.13417.

{[Rh(*t*-Bu-BisP*)H]$_3$(μ_2-H)$_3$(μ_3-H)}(BF$_4$)$_2$

[Rh(*t*-Bu-BisP*)(nbd)]BF$_4$ (0.02mmol) was dissolved in 1 mL *i*-PrOH under an argon atmosphere. The argon atmosphere was exchanged by hydrogen and the solution stirred under hydrogen normal pressure for 0.5 h. The solution was allowed to stand without stirring. Already after a few hours yellow crystals were isolated, which were washed with diethyl ether and dried under vacuum.

MS (ESI-TOF): calc for {[Rh(*t*-Bu-BisP*)H]$_3$(μ_2-H)$_3$(μ_3-H)}$^{2+}$; ($C_{36}H_{91}P_6Rh_3$): 509.13503; found: 509.13589.

IR: see figure S1.

Raman: see figure S2.

1.2. IR-and Raman spectra

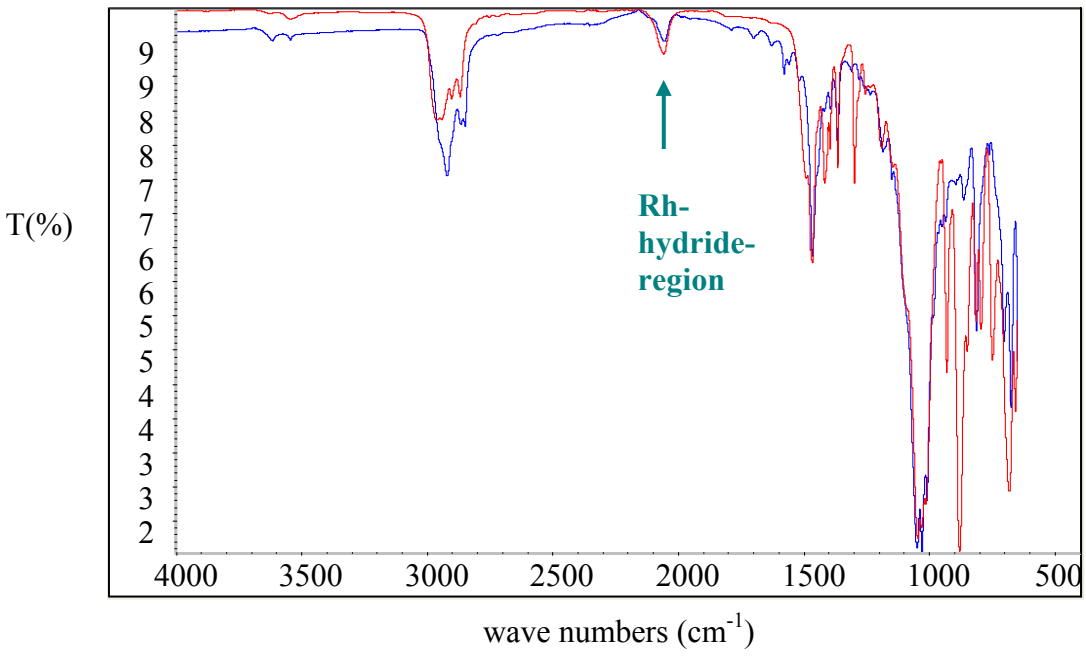

Fig. S1 IR spectra of {[Rh(*t*-Bu-BisP*)H]$_3$(μ_2-H)$_3$(μ_3-H)}(BF$_4$)$_2$ (red) and {[Rh(Tangphos)H]$_3$(μ_2-H)$_3$(μ_3-H)}(BF$_4$)$_2$ (blue).

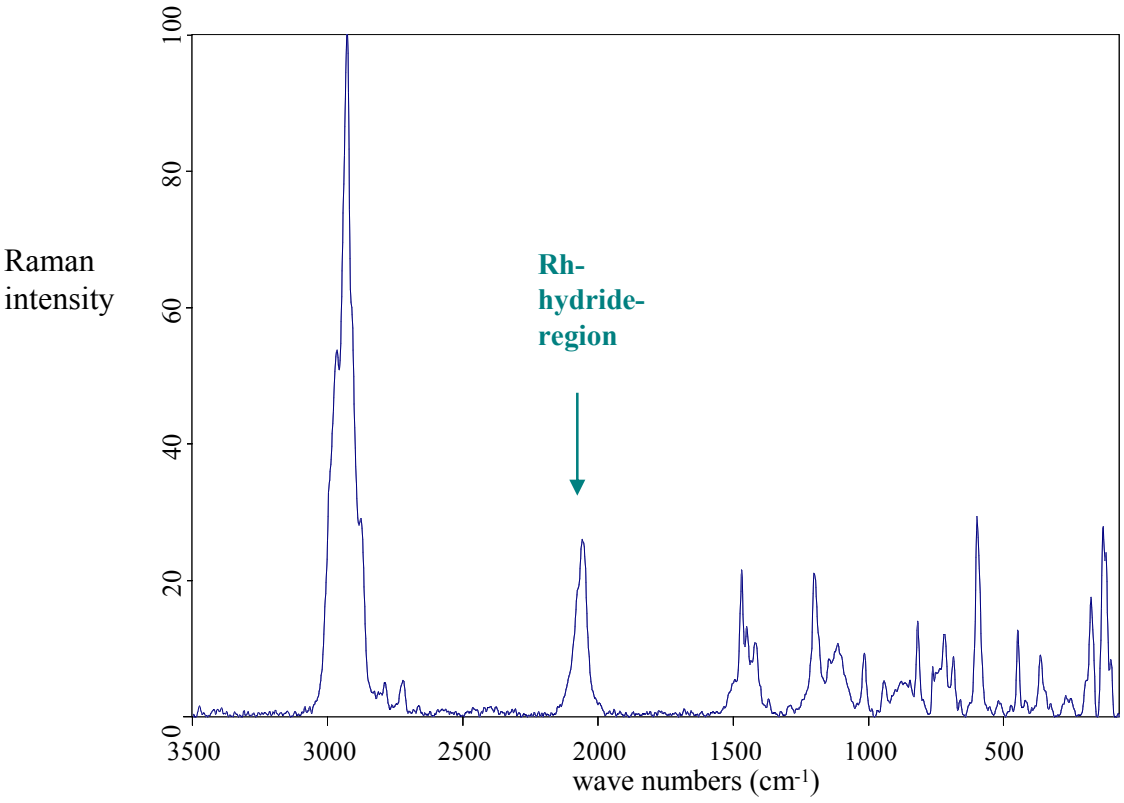

Fig. S2 Raman spectra of $\{[Rh(t\text{-Bu-BisP*})H]_3(\mu_2\text{-}H)_3(\mu_3\text{-}H)\}(BF_4)_2$.

1.3.Additional NMR-spectra

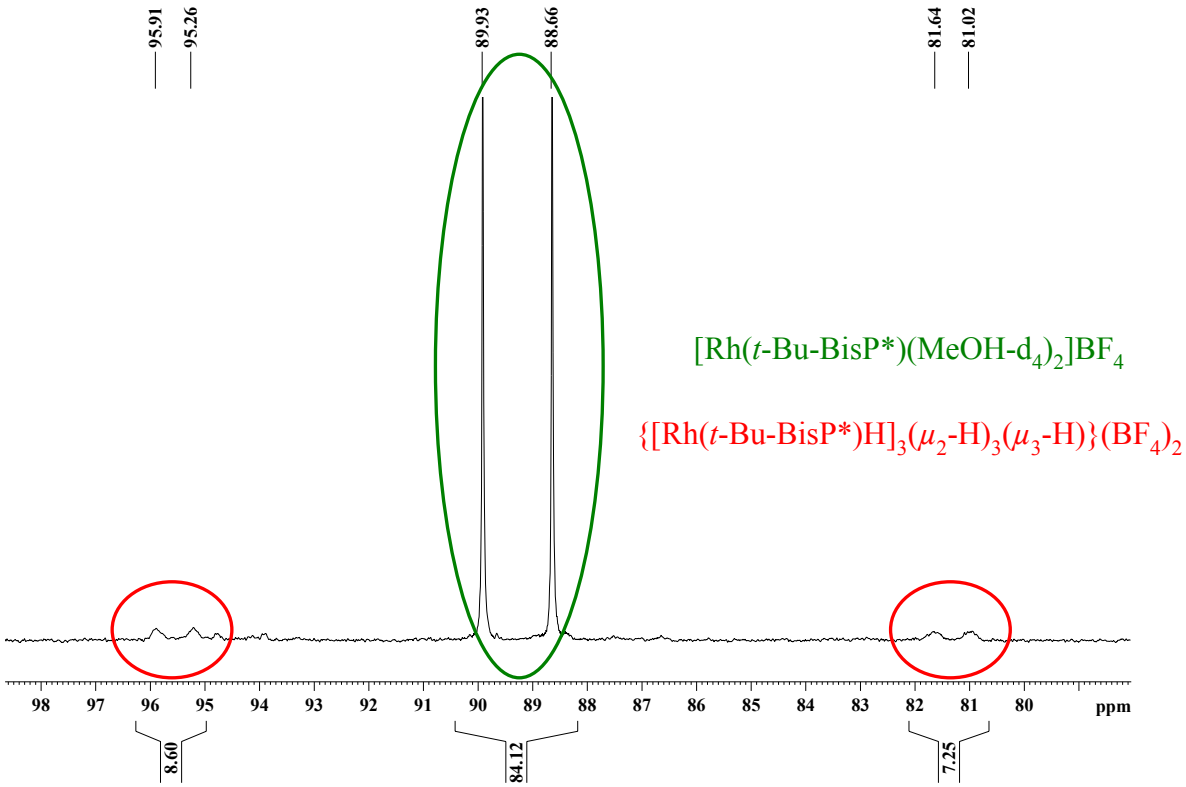

Fig. S3 ^{31}P NMR spectrum of [Rh(*t*-Bu-BisP*)(nbd)]BF_4 after complete hydrogenation of the diolefin in methanol-d_4. The signals of the trinuclear hydride complex started to appear after ca. 15 hours.

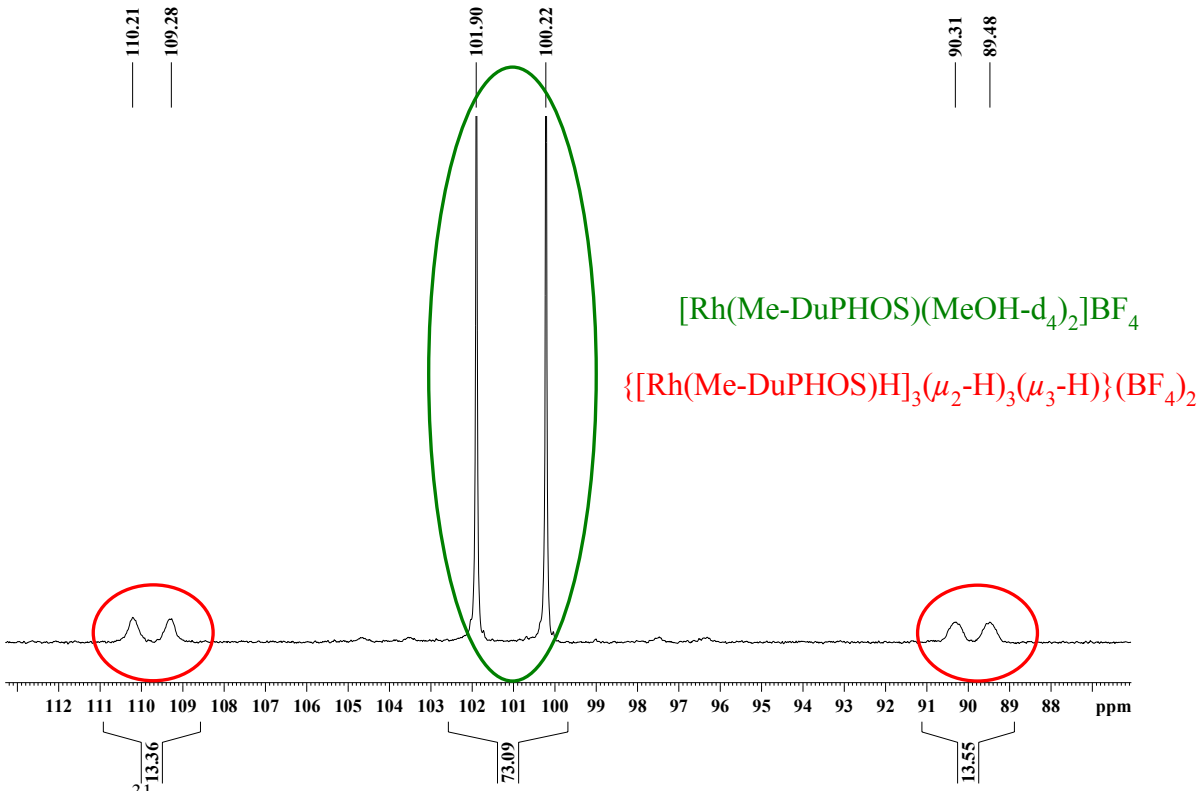

Fig. S4 ^{31}P NMR spectrum of [Rh(Me-DuPHOS)(nbd)]BF_4 after complete hydrogenation of the diolefin in methanol-d_4. The signals of the trinuclear hydride complex started to appear after ca. 14 days.

^{1}H NMR spectra of Rh complexes

The core of the complex, $Rh_3H_7P_6$, is built from sixteen nuclei with I = ½, spin-spin coupling leads to complicated line patterns. Each of the protons couples to the heteronuclei and to the other protons of the core due to their magnetic inequivalence, and furthermore there are scalar couplings to the protons of the ligand backbones (e. g. ^{1}H COSY correlations found for the *t*-Bu-BisP* complex: –9.05 ppm/1.86 ppm and 2.05 ppm, –15.72 ppm/1.86 ppm and 2.55 ppm). Therefore, spectra are of higher order and cannot be analysed by simple multiplicity rules. However, if we decouple phosphorus, the sixteen-spin system is reduced to ten-spin Rh_3H_7 and may, if we consider the small H-H couplings between hydrides and ligand backbone protons not relevant for the appearance of the signals, approximated by first-order patterns. For the following analysis we assume that the multiplicity patterns in the ^{1}H{^{31}P} spectra are dominated by rhodium-hydrogen scalar coupling.

The hydride signal of lowest intensity, a multiplet of ten lines, collapses to a regular quartet and is therefore assigned to a proton coupling to three rhodium atoms in the same manner. This must be the μ_3-hydrogen. The fine structure of the quartet lines (septet structure?) could be due to coupling to the other six hydride ligands, if coupling constants to terminal and bridging ones are similar (the observed splitting is about 3.1 to 3.4 Hz). The ten-line pattern in the phosphorus-coupled spectra is less straightforward explicable, however, if we consider the coordination sphere around the Rh(III) as roughly octahedral, we find that the μ_3-H has three transoid P atoms (designated P2, P4, P6 in the structure of the Tangphos complex), we expect three large coupling constants. With the assumption $^2J_{P,H} \approx 2 \cdot {}^1J_{Rh,H}$ (see captions to Figures S5, S6, S7) we would get a quartet of quartets which is built from ten lines (albeit the expected intensity distribution does not really match the observed).

The hydride signal with highest frequency appears as a doublet of unresolved triplets and represents three nuclei. It collapses to a well-resolved triplet and should therefore be assigned the bridging (μ_2) hydrogen. Each of these bridges has exactly one transoid P atom (designated P1, P3, P5 in the structure of the Tangphos complex) that causes the large splitting up to 99 Hz by $^2J_{P(trans),H}$. Other couplings ($^2J_{P(cis),H}$, $^2J_{H,H}$) are considerably smaller and not resolved.
The hydride signal with lowest frequency appears as six-line pattern and represents three nuclei. It collapses to a doublet and should therefore be assigned terminal (σ) hydrogen. The origin of the six-line pattern is not yet clear. The observed intensities (1:4:5:5:4:1) may account for a doublet of quartets (with $J_d = 2 \cdot J_q$), but as the terminal H have only two cisoid P atoms in their environment and there are no resolved H,H couplings, the origin of the large doublet coupling remains unexplained. We should however keep in mind that the simple interpretation presented here is not correct in a strict sense because we are dealing with a large, strongly coupled spin system.

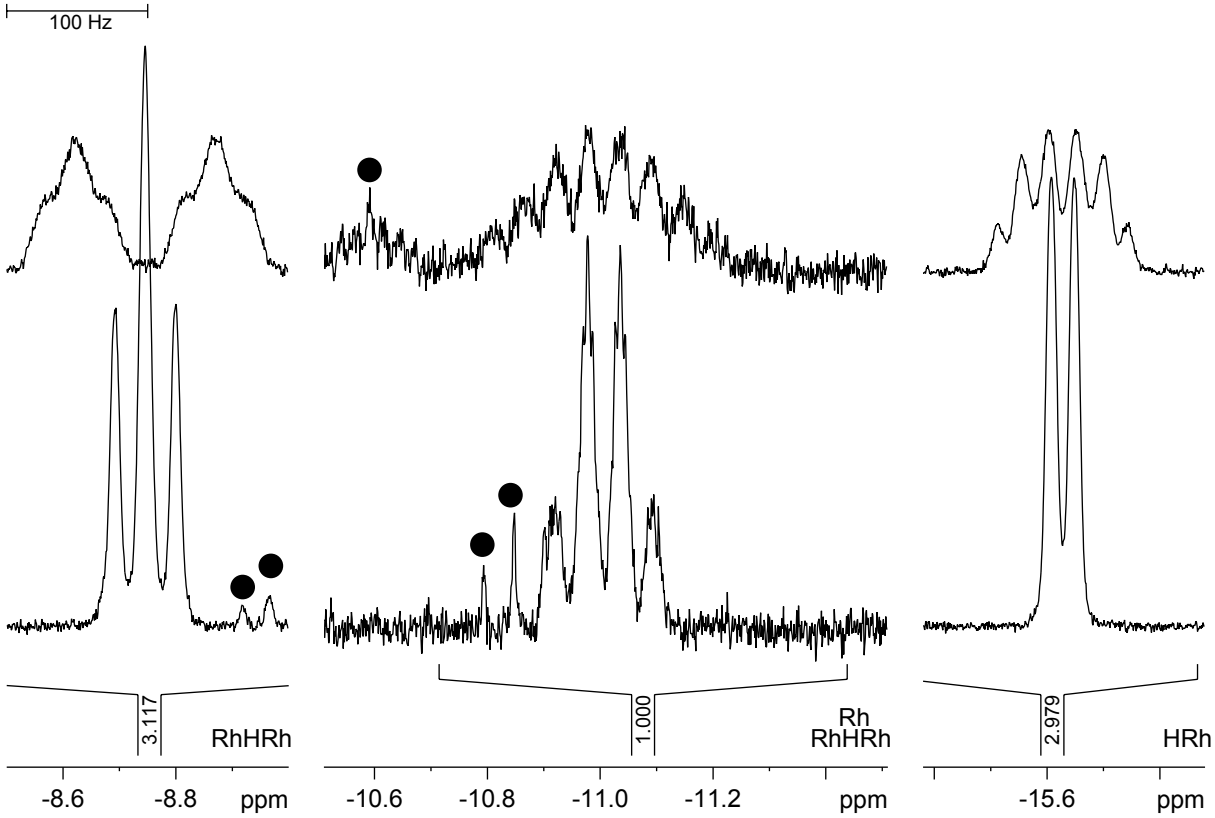

Fig. S5 ^{1}H NMR spectra (400.13 MHz, hydride region) of {[Rh(Tangphos)H]$_3$(μ_2-H)$_3$(μ_3-H)}[BF$_4$]$_2$ in CD_2Cl_2 at ambient temperature. Top trace: phosphorus-coupled, bottom trace: phosphorus-decoupled. Chemical shifts: 2.8 to 1.5 ppm, CH and CH_2 of phospholane, not further analysed; 1.17 ppm (d, 27 H, *t*-Bu, $^3J_{P,H}$ 15 Hz); 1.06 ppm (d, 27 H, *t*-Bu, $^3J_{P,H}$ 15 Hz); –8.75 ppm (dt, 3 H, μ_2-H, $^1J_{Rh,H}$ 21.8 Hz, $^2J_{P,H}$ 99 Hz); –11.01 ppm (m, 1 H, μ_3-H, $^1J_{Rh,H}$ 23.2 Hz, $^2J_{P,H}$ presumably about 46 Hz, see text); –15.63 ppm (3 H, σ-H, $^1J_{Rh,H}$ 16.2 Hz, see text). The dots are due to impurities.

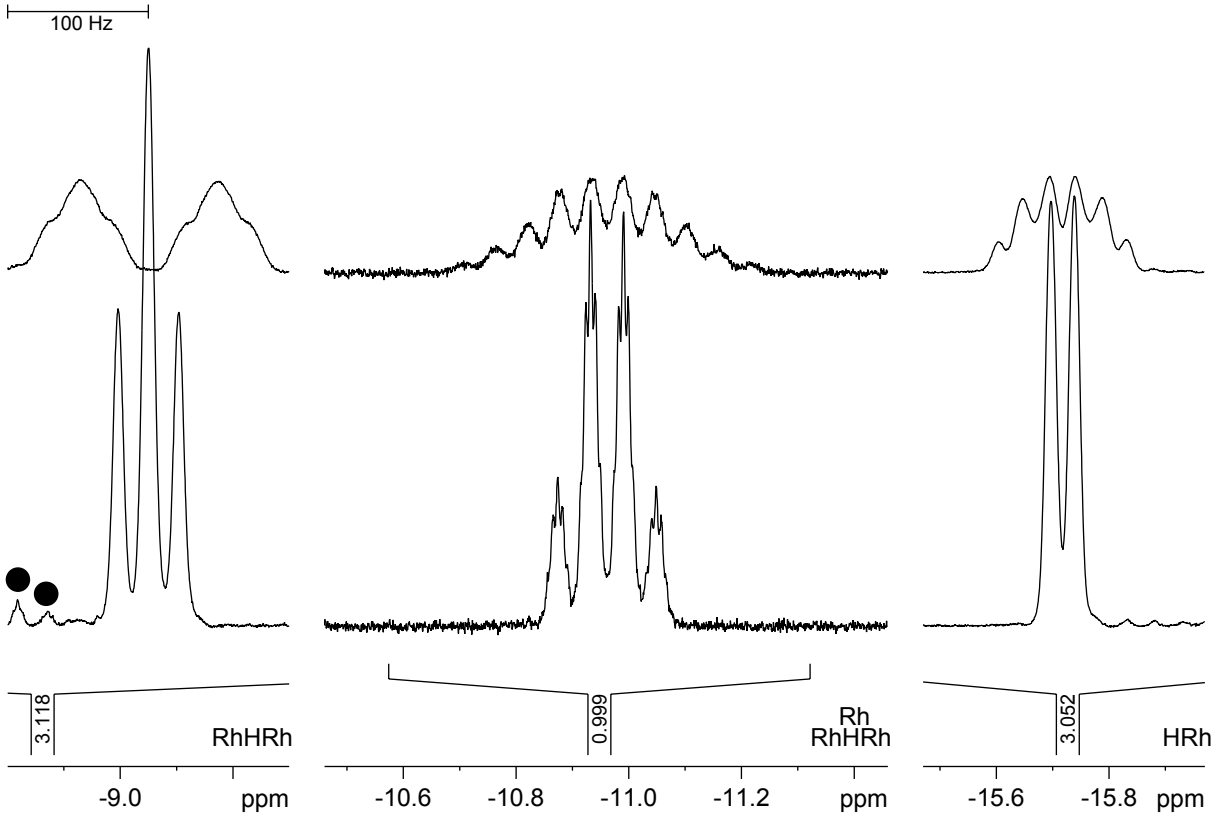

Fig. S6 ^{1}H NMR spectra (400.13 MHz, hydride region) of {[Rh(*t*-Bu-BisP*)H]$_3$(μ_2-H)$_3$(μ_3-H)}[BF_4]$_2$ in CD_2Cl_2 at ambient temperature. Top trace: phosphorus-coupled, bottom trace: phosphorus-decoupled. Chemical shifts: 2.55 ppm (m, 3 H of CH_2); 2.32 ppm (m, 3 H of CH_2); 2.05 (d, 9 H, $^{2}J_{P,H}$ 9 Hz, CH_3 at P_{trans}); 1.89 ppm (m, 6 H of CH_2); 1.86 (d, 9 H, $^{2}J_{P,H}$ 10 Hz, CH_3 at P_{cis}); 1.15 ppm (d, 27 H, *t*-Bu at P_{cis}, $^{3}J_{P,H}$ 15 Hz); 1.05 ppm (d, 27 H, *t*-Bu at P_{trans}, $^{3}J_{P,H}$ 15 Hz); –9.05 ppm (dt, 3 H, μ_2-H, $^{1}J_{Rh,H}$ 21.6 Hz, $^{2}J_{P,H}$ 98 Hz); –10.96 ppm (m, 1 H, μ_3-H, $^{1}J_{Rh,H}$ 23.3 Hz, $^{2}J_{P,H}$ presumably about 46 Hz, see text); –15.72 ppm (3 H, σ-H, $^{1}J_{Rh,H}$ 16.6 Hz, see text). The dots are due to impurities.

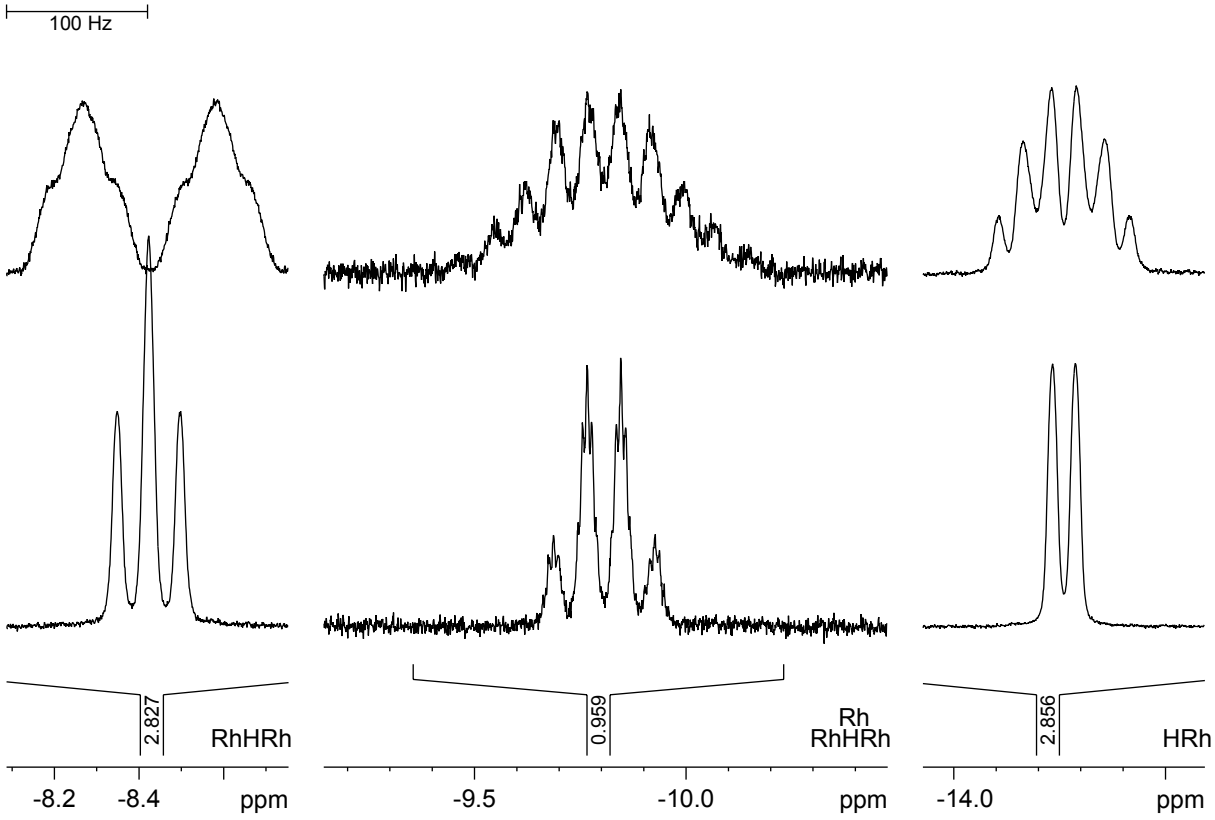

Fig. S7 ^{1}H NMR spectra (300.13 MHz, hydride region) of {[Rh(Me-DuPhos)H]$_3$(μ_2-H)$_3$(μ_3-H)}[BF$_4$]$_2$ in CD_2Cl_2 at ambient temperature. Top trace: phosphorus-coupled, bottom trace: phosphorus-decoupled. Chemical shifts: 7.84 ppm (m, 3 H arom.); 7.77 ppm (m, 9 H arom.); 3.72 ppm (m, 3 H phospholane); 2.93 ppm (m, 3 H phospholane); 2.7 to 2.2 ppm (m, 18 H phospholane); 1.94 ppm (m, 3 H phospholane); 1.79 ppm (m, 3 H phospholane); 1.50 ppm (m, 6 H phospholane); 1.23 ppm (dd, 9 H, $^{2}J_{P,H}$ 18.9 Hz, $^{3}J_{H,H}$ 6.7 Hz, CH_3); 1.19 ppm (dd, 9 H, $^{2}J_{P,H}$ 18.8 Hz, $^{3}J_{H,H}$ 7.1 Hz, CH_3); 1.08 ppm (dd, 9 H, $^{2}J_{P,H}$ 17.4 Hz, $^{3}J_{H,H}$ 7.0 Hz, CH_3); 0.70 ppm (dd, 9 H, $^{2}J_{P,H}$ 15.6 Hz, $^{3}J_{H,H}$ 7.1 Hz, CH_3); –8.42 ppm (dt, 3 H, μ_2-H, $^{1}J_{Rh,H}$ 22.4 Hz, $^{2}J_{P,H}$ 94 Hz); –9.81 ppm (m, 1 H, μ_3-H, $^{1}J_{Rh,H}$ 24.0 Hz, $^{2}J_{P,H}$ presumably about 46 Hz, see text); –14.26 ppm (3 H, σ-H, $^{1}J_{Rh,H}$ 16.2 Hz, see text).

2. Crystallographic Section

2.1. Crystallographic experimental section

Crystal data and details of the structure solution are summarised in table S1. Diffraction data were collected on a STOE-IPDS II diffractometer using graphite monochromated Mo-Kα radiation. The structure were solved by direct methods (SHELXS-97)[1] and refined by full matrix least square techniques against F^2 (SHELXL-97)[1]. XP (Siemens Analytical X-ray Instruments, Inc.) was used for structure representations.

The nonhydrogen atoms, except the partially occupied atoms, were refined anisotropically. The hydrogen atoms, except the hydrides, were placed into theoretical positions and were refined by using the riding model. The weighting schemes used in the last cycles of refinement are are $\omega = 1/[\sigma^2(Fo^2) + (0.0754P)^2 + 0.0000P]$ for [Rh((*S,S,R,R*)-Tangphos)(cod)]BF_4, $\omega = 1/[\sigma^2(Fo^2) + (0.0754P)^2 + 0.1294P]$ for [Rh((*S,S,R,R*)-Tangphos)(nbd)]BF_4+thf, $\omega = 1/[\sigma^2(Fo^2) + (0.0557P)^2 + 0.0000P]$ for [Rh((*R,R*)-*t*-Bu-BisP*)(cod)]BF_4 [2], $\omega = 1/[\sigma^2(Fo^2) + (0.0410P)^2 + 0.0000P]$ for {[Rh((*R,R*)-*t*-Bu-BisP*)H]$_3$(μ_2-H)$_3$(μ_3-H)}$(BF_4)_2$*½ *i*-PrOH [2], $\omega = 1/[\sigma^2(Fo^2) + (0.0000P)^2 + 0.0000P]$ for {[Rh((*S,S*)-Me-DuPHOS)H]$_3$(μ_2-H)$_3$(μ_3-H)}$(BF_4)_2$*2 EtOEt, $\omega = 1/[\sigma^2(Fo^2) + (0.0.0506P)^2 + 0.0000P]$ for {[Rh((*S,S,R,R*)-Tangphos)H]$_3$(μ_2-H)$_3$(μ_3-H)}$(BF_4)_2$*MeOH, $\omega = 1/[\sigma^2(Fo^2) + (0.0360P)^2 + 0.0000P]$ for {[Rh((*S,S,R,R*)-Tangphos)H]$_3$(μ_2-H)$_3$(μ_3-H)}$(BF_4)_2$*2 CH_2Cl_2 and $\omega = 1/[\sigma^2(Fo^2) + (0.0720P)^2 + 0.0000P]$ for {[Rh((*S,S,R,R*)-Tangphos)H]$_3$(μ_2-H)$_3$(μ_3-H)}$(BF_4)_2$ * ½ toluene.

Crystallographic datas (excluding structure factors) for the structures reported in this paper have been deposited at the Cambridge Crystallographic Data Centre as supplementary publication no. CCDC-793506 for [Rh((*S,S,R,R*)-Tangphos)(cod)]BF_4, CCDC-793500 for [Rh((*S,S,R,R*)-Tangphos)(nbd)]BF_4*thf, CCDC-793505 for [Rh((*R,R*)-*t*-Bu-BisP*)(cod)]BF_4, CCDC-793504 for {[Rh((*R,R*)-*t*-Bu-BisP*)H]$_3$(μ_2-H)$_3$(μ_3-H)}$(BF_4)_2$*½ *i*-PrOH , CCDC-793499 for {[Rh((*S,S*)-Me-DuPHOS)H]$_3$(μ_2-H)$_3$(μ_3-H)}$(BF_4)_2$*2 EtOEt, CCDC-793501 for {[Rh((*S,S,R,R*)-Tangphos)H]$_3$(μ_2-H)$_3$(μ_3-H)}$(BF_4)_2$*MeOH, CCDC-793502 for {[Rh((*S,S,R,R*)-Tangphos)H]$_3$(μ_2-H)$_3$(μ_3-H)}$(BF_4)_2$*2 CH_2Cl_2 and CCDC-793503 for {[Rh((*S,S,R,R*)-Tangphos)H]$_3$(μ_2-H)$_3$(μ_3-H)}$(BF_4)_2$ * ½ toluene. Copies of the data can be obtained free of charge on application to CCDC, 12 Union Road, Cambridge, CB21EZ, UK (fax: int. code + (1223) 336-033; e-mail: deposit@ccdc.cam.ac.uk.

[1] G. M. Sheldrick, *Acta Cryst. A* **1997** *64*, 112-122.
[2] The quality is just enaugh for the proof of the structure and cannot be used for any geometrical discussion.

Table S1 Crystallographic and refinement data for [Rh((*S,S,R,R*)-Tangphos)(nbd)]BF_4*THF, [Rh((*S,S,R,R*)-Tangphos)(cod)]BF_4, [Rh((*R,R*)-*t*-Bu-BisP*)(cod)]BF_4, {[Rh((*R,R*)-*t*-Bu-BisP*)H]$_3$(μ_2-H)$_3$(μ_3-H)}$(BF_4)_2$*½ *i*-PrOH, {[Rh((*S,S*)-Me-DuPHOS)H]$_3$(μ_2-H)$_3$(μ_3-H)}$(BF_4)_2$*2 EtOEt, {[Rh((*S,S,R,R*)-Tangphos)H]$_3$(μ_2-H)$_3$(μ_3-H)}$(BF_4)_2$*MeOH, {[Rh((*S,S,R,R*)-Tangphos)H]$_3$(μ_2-H)$_3$(μ_3-H)}$(BF_4)_2$*2 CH_2Cl_2 and {[Rh((*S,S,R,R*)-Tangphos)H]$_3$(μ_2-H)$_3$(μ_3-H)}$(BF_4)_2$ * ½ toluene

Compound	[Rh((*S,S,R,R*)-Tangphos)(nbd)]BF_4*thf	[Rh((*S,S,R,R*)-Tangphos)(cod)]BF_4
Empirical formula	$C_{27}H_{48}BF_4OP_2Rh$	$C_{24}H_{44}BF_4P_2Rh$
Formula weight	640.31	584.25
Crystal system	monoclinic	monoclinic
Space group	P*2$_1$*	C*2*
a [Å]	9.7263 (19)	18.240 (4)
b [Å]	14.776 (3)	8.0358 (16)
c [Å]	10.458 (2)	19.188 (4)
α [°]	90	90
β [°]	107.72 (3)	109.06 (3)
γ [°]	90	90
V [Å^3]	1431.6 (5)	2658.3 (9)
d_c [Mg/m^3]	1.485	1.460
Z	2	4
μ [mm^{-1}]	0.754	0.801
F(000)	668	1216
Crystal size [mm]	0.50 x 0.37 x 0.25	0.50 x 0.35 x 0.30
Temperature [K]	150	200
Scan range (2Θ) [°]	4.08 – 53.00	4.50 – 55.80
Index range (hkl)	-11/12, -18/18, -13/13	-23/24, -10/10, -25/25
Reflection collected	21863	22973
Independent reflections	5946	6252
Observed reflections	5873	5793
parameters	325	289
R1 (int)	0.0203	0.0610
R1 (2σ(I))	0.0184	0.0351
R1 (all data)	0.0187	0.0376
wR2 (all data)	0.0501	0.0967
Goodness of fit	1.034	1.009
Flack parameter	-0.020 (14)	-0.01 (3)
Largest difference peak and hole (e/ Å)	0.46/-0.36	1.03/-0.97

Compound	[Rh((*R,R*)-*t*-Bu-BisP*)(cod)]BF_4	{[Rh((*R,R*)-*t*-Bu-BisP*)H]$_3$ (μ_2-H)$_3$(μ_3-H)}$(BF_4)_2$*½ *i*-PrOH
Empirical formula	$C_{20}H_{40}BF_4P_2Rh$	$C_{37.5}H_{95}B_2F_8O_{0.5}P_6Rh_3$
Formula weight	532.18	1222.31
Crystal system	monoclinic	monoclinic
Space group	C*2*	P*2$_1$*
a [Å]	18.684 (2)	11.215 (4)
b [Å]	7.606 (6)	12.336 (2)
c [Å]	17.408 (2)	21.365 (4)
α [°]	90	90
β [°]	92.781 (9)	100.37 (3)
γ [°]	90	90
V [Å^3]	2470.8 (5)	2907.5 (10)
d_c [Mg/m^3]	1.431	1.396
Z	4	2
μ [mm^{-1}]	0.854	1.057
F(000)	1104	1262
Crystal size [mm]	0.20 x 0.15 x 0.10	0.40 x 0.20 x 0.20
Temperature [K]	200	200
Scan range (2Θ) [°]	4.36 – 51.00	3.70 – 50.22
Index range (hkl)	-21/22, -9/6, -21/21	-13/12, -14/14, -25/25
Reflection collected	5159	33342
Independent reflections	3320	10001
Observed reflections	2598	7296
parameters	234	532
R1 (int)	0.0269	0.0498
R1 (2σ(I))	0.0491	0.0473
R1 (all data)	0.0658	0.0646
wR2 (all data)	0.1151	0.1054
Goodness of fit	1.193	0.905
Flack parameter	0.00 (9)	-0.01 (4)
Largest difference peak and hole (e/ Å)	1.40/-0.66	0.86/-0.58

Compound	{[Rh((*S,S*)-Me-DuPHOS)H]$_3$ (μ_2-H)$_3$(μ_3-H)}(BF$_4$)$_2$*2 EtOEt,	{[Rh((*S,S,R,R*)-Tangphos)H]$_3$ (μ_2-H)$_3$ (μ_3-H)}(BF$_4$)$_2$*MeOH
Empirical formula	$C_{62}H_{111}B_2F_8O_2P_6Rh_3$	$C_{49}H_{107}B_2F_8OP_6Rh_3$
Formula weight	1556.62	1380.46
Crystal system	orthorhombic	orthorhombic
Space group	$P2_12_12_1$	$P2_12_12_1$
a [Å]	14.2607 (5)	11.2487 (2)
b [Å]	22.1231 (9)	20.2463 (2)
c [Å]	23.0014 (8)	28.4783 (4)
α [°]	90	90
β [°]	90	90
γ [°]	90	90
V [Å^3]	7256.7 (5)	6485.78 (16)
d_c [Mg/m^3]	1.425	1.414
Z	4	4
μ [mm^{-1}]	0.866	0.957
F(000)	3252	2892
Crystal size [mm]	0.25 x 0.20 x 0.15	0.20 x 0.20 x 0.15
Temperature [K]	200	200
Scan range (2Θ) [°]	3.36 – 51.38	3.50 – 53.50
Index range (hkl)	-17/17, -26/26, -27/28	-14/14, -25/25, -35/35
Reflection collected	77805	71877
Independent reflections	13644	13762
Observed reflections	8792	11697
parameters	743	641
R1 (int)	0.0966	0.0384
R1 (2σ(I))	0.0561	0.0354
R1 (all data)	0.0899	0.0438
wR2 (all data)	0.1134	0.0836
Goodness of fit	0.943	0.943
Flack parameter	-0.02 (4)	-0.02 (3)
Largest difference peak and hole (e/ Å)	1.03-081	0.96/-0.70

Compound	{[Rh((*S,S,R,R*)-Tangphos)H]$_3$ (μ_2-H)$_3$(μ_3-H)}(BF$_4$)$_2$ *2 CH_2Cl_2	{[Rh((*S,S,R,R*)-Tangphos)H]$_3$ (μ_2-H)$_3$(μ_3-H)}(BF$_4$)$_2$ * ½ toluene
Empirical formula	$C_{50}H_{107}B_2Cl_4F_8P_6Rh_3$	$C_{51.5}H_{107}B_2F_8P_6Rh_3$
Formula weight	1518.27	1394.48
Crystal system	orthorhombic	orthorhombic
Space group	$P2_12_12_1$	$P2_12_12_1$
a [Å]	11.3450 (2)	11.3053 (2)
b [Å]	20.2993 (2)	20.2980 (2)
c [Å]	28.8790 (4)	28.9060 (4)
α [°]	90	90
β [°]	90	90
γ [°]	90	90
V [Å^3]	6650.89 (16)	6633.20 (16)
d_c [Mg/m^3]	1.516	1.396
Z	4	4
μ [mm^{-1}]	1.095	0.936
F(000)	3156	2920
Crystal size [mm]	0.20 x 0.15 x 0.15	0.50 x 0.25 x 0.10
Temperature [K]	200	200
Scan range (2Θ) [°]	2.82 – 53.50	2.82 – 53.48
Index range (hkl)	-14/14. -25/25. -36/36	-14/13. -25/25. -36/36
Reflection collected	101570	102604
Independent reflections	14110	14063
Observed reflections	11672	12183
parameters	674	636
R1 (int)	0.0590	0.0407
R1 (2σ(I))	0.0311	0.0369
R1 (all data)	0.0399	0.0430
wR2 (all data)	0.0683	0.1041
Goodness of fit	0.901	0.960
Flack parameter	-0.02 (2)	-0.03 (3)
Largest difference peak and hole (e/ Å)	0.84/-0.67	1.65/-0.56

2.2. Figures of the molecul structures

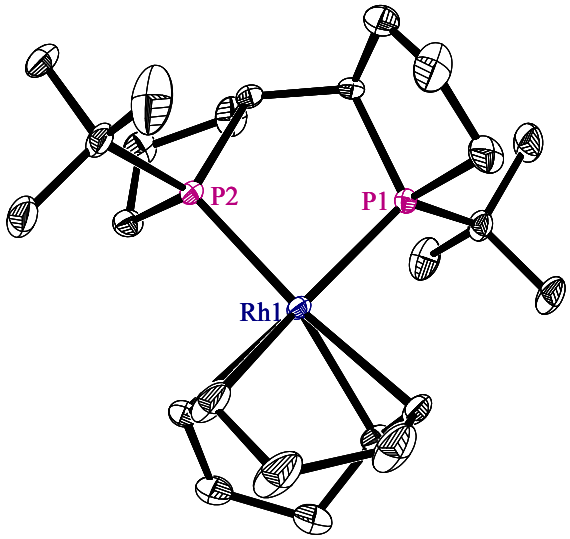

Fig. S8 Molecular structure of the cation [Rh((*S,S,R,R*)-Tangphos)(cod)]$^+$; ORTEP, 30 % probability ellipsoids. Hydrogen atoms are omitted for clarity. Selected distances [Å] and angles [°]: Rh-P 2.299(1)-2.297(1); Rh-C 2.208(5)-2.258(5); P-Rh-P 85.61(4).

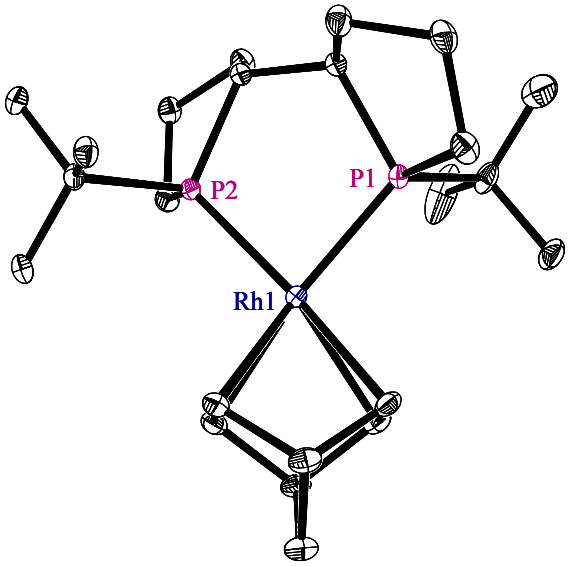

Fig. S9 Molecular structure of the cation [Rh((*S,S,R,R*)-Tangphos)(nbd)]$^+$; ORTEP, 30 % probability ellipsoids. Hydrogen atoms are omitted for clarity. Selected distances [Å] and angles [°]: Rh-P 2.294-2.297; Rh-C 2.196-2.221; P-Rh-P 85.05.

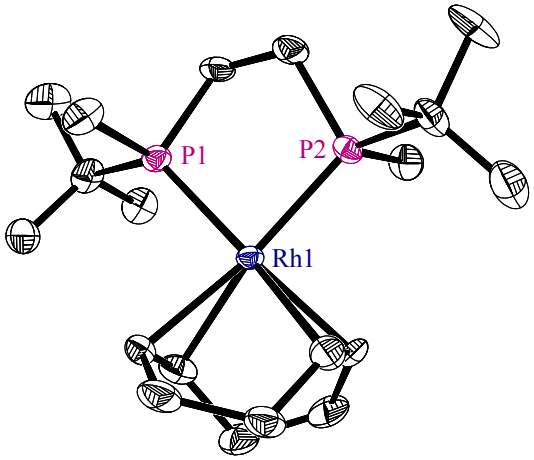

Fig. S10 Molecular structure of the cation [Rh((*R,R*)-*t*-Bu-BisP*)(cod)]$^{+}$. ORTEP, 30 % probability ellipsoids. Hydrogen atoms are omitted for clarity. Selected distances [Å] and angles [°]: Rh-P 2.289(1)-2.295(1); Rh-C 2.194(5)-2.260(5); P-Rh-P 83.92(4).

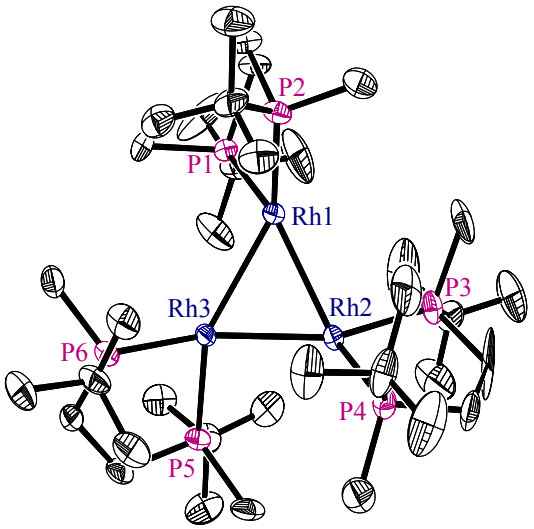

Fig. S11 Molecular structure of $\{[Rh((R,R)\text{-}t\text{-Bu-BisP*})H]_3(\mu_2\text{-}H)_3(\mu_3\text{-}H)\}^{2+}$; ORTEP, 30 % probability ellipsoids. Hydrides could not be refined. Rh-Rh 2.772-2.793 Å.

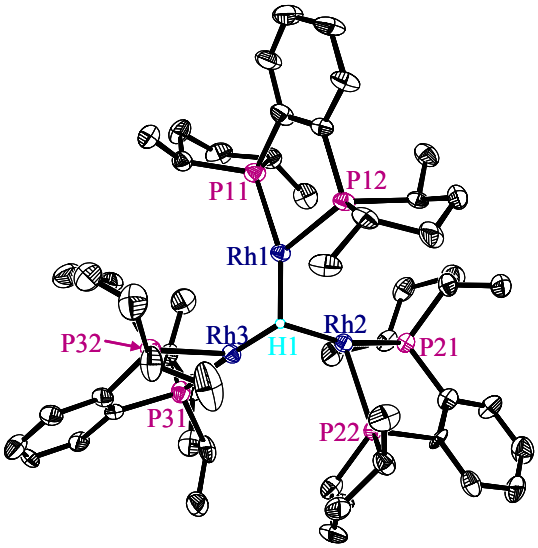

Fig. S12 Molecular structure of $\{[Rh((S,S)\text{-Me-DuPHOS})H]_3(\mu_2\text{-}H)_3(\mu_3\text{-}H)\}^{2+}$; ORTEP, 30 % probability ellipsoids. Hydrides, with the exception of the μ_3-bridging one, could not be refined. Rh-Rh 2,776-2,790 Å.

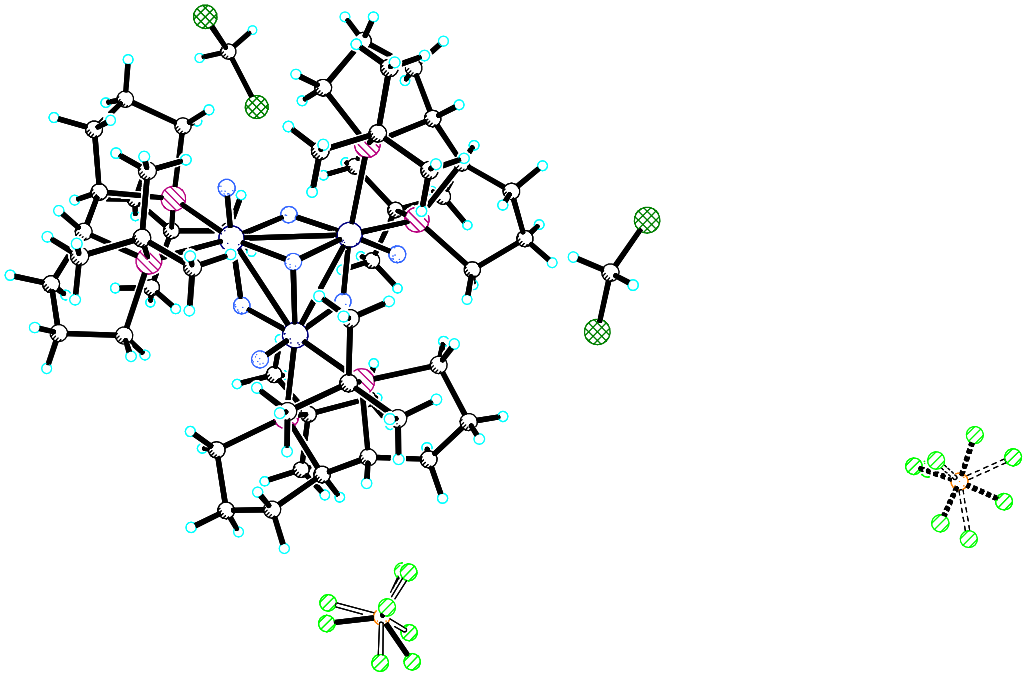

Fig. S13: Molecular structure of {[Rh((*S,S,R,R*)-Tangphos)H]$_3$(μ_2-H)$_3$(μ_3-H)}(BF$_4$)$_2$*2 CH_2Cl_2 crystallized from dichloromethane. Hydride positions were calculated from the known positions of the isomorphic {[Rh((*S,S,R,R*)-Tangphos)H]$_3$(μ_2-H)$_3$(μ_3-H)}(BF$_4$)$_2$*MeOH and fixed by restraints.

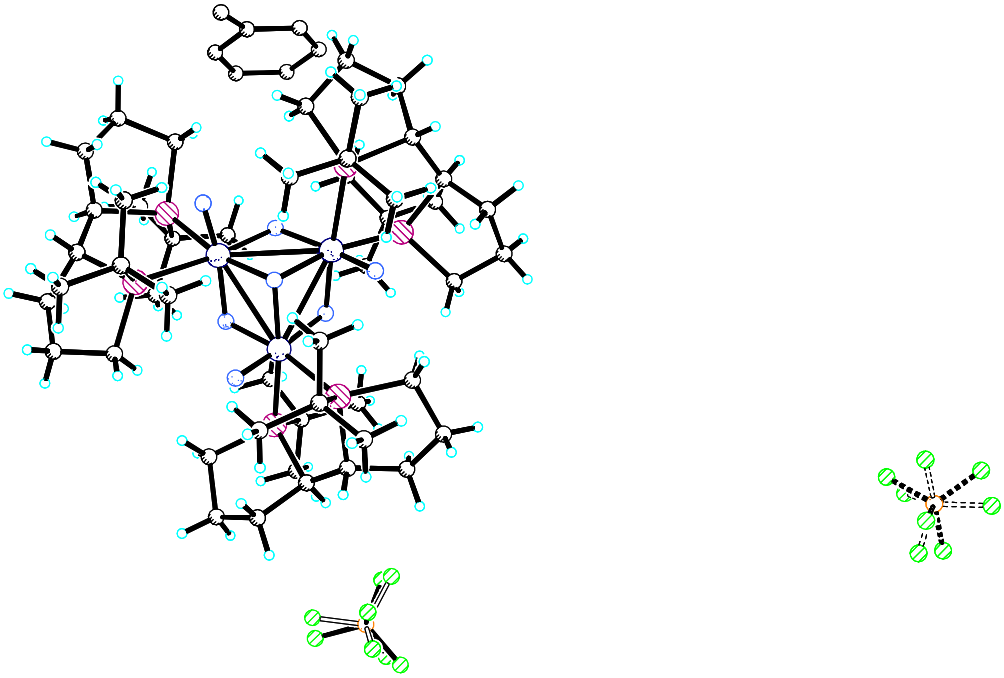

Fig. S14 Molecular structure of {[Rh((*S,S,R,R*)-Tangphos)H]$_3$(μ_2-H)$_3$(μ_3-H)}(BF$_4$)$_2$*1 toluene crystallized from toluene. Hydride positions were calculated from the known positions of the isomorphic {[Rh((*S,S,R,R*)-Tangphos)H]$_3$(μ_2-H)$_3$(μ_3-H)}(BF$_4$)$_2$*MeOH and fixed by restraints.